JOURNAL OF GEOPHYSICAL RESEARCH, VOL. 106, NO. D24, PAGES 33,761–33,772, DECEMBER 27, 2001

Coherent radar ice thickness measurements over the Greenland ice sheet

S. Gogineni,[1] D. Tammana,[1] D. Braaten,[1] C. Leuschen,[1] T. Akins,[2] J. Legarsky,[3] P. Kanagaratnam,[1] J. Stiles,[1] C. Allen,[1] and K. Jezek[4]

Abstract. We developed two 150-MHz coherent radar depth sounders for ice thickness measurements over the Greenland ice sheet. We developed one of these using connectorized components and the other using radio frequency integrated circuits (RFICs). Both systems are designed to use pulse compression techniques and coherent integration to obtain the high sensitivity required to measure the thickness of more than 4 km of cold ice. We used these systems to collect radar data over the interior and margins of the ice sheet and several outlet glaciers. We operated both radar systems on the NASA P-3B aircraft equipped with GPS receivers. Radar data are tagged with GPS-derived location information and are collected in conjunction with laser altimeter measurements. We have reduced all data collected since 1993 and derived ice thickness along all flight lines flown in support of Program for Regional Climate Assessment (PARCA) investigations and the North Greenland Ice Core Project. Radar echograms and derived ice thickness data are placed on a server at the University of Kansas (http://tornado.rsl.ukans.edu/Greenlanddata.htm) for easy access by the scientific community. We obtained good ice thickness information with an accuracy of ±10 m over 90% of the flight lines flown as a part of the PARCA initiative. In this paper we provide a brief description of the system along with samples of data over the interior, along the 2000-m contour line in the south and from a few selected outlet glaciers.

1. Introduction

In 1991, NASA started a polar research initiative aimed at determining the mass balance of the Greenland ice sheet. This program consisted of coordinated surface, airborne, and spaceborne measurements for determining the mass balance of the ice sheet. The initial airborne program consisted of a laser altimeter and a Ku-band radar altimeter for measuring surface elevation of the ice sheet along selected flight lines. In 1993 the airborne instrumentation suite was expanded to include a radar depth sounder to collect ice thickness data along the same flight lines. Ice thickness is a key variable in the time-dependent equation of continuity and is essential to any study of ice sheet dynamics.

Raju et al. [1990] developed a coherent radar sounder for measurements in the Antarctic. We used this system to collect ice thickness data during the 1993 field season. Although the system collected good quality data in certain areas in the north and central parts of the ice sheet, its performance was less than optimum for obtaining ice thickness data over a few parts of the ice sheet in southern Greenland. These are in temperate areas of the ice sheet with thick, warm ice. To overcome its limitations and improve its performance, we developed two new systems: one using connectorized components and the other using radio frequency integrated circuits (RFICs). The transmitter and receiver prototypes for the system using RFICs were developed by senior undergraduate students as part of a capstone design project. We used these prototypes to develop an operational system that was used to collect some of the data reported in this paper.

Both radar systems operate at the center frequency of 150 MHz with a chirped pulse of 1.6 μs duration and peak transmit power of about 200 W. We also applied the frequency-wavenumber (*f-k*) migration algorithm [*Gazdag and Sguazzero*, 1984; *Stolt*, 1978] to process a few selected data sets to improve signal-to-noise (S/N) ratio and resolution. We have placed all of the ice thickness data, including radio echograms and ice thicknesses derived from these echograms, on a server for the science community to download and use in their research. These data from two nearly identical radars cover over 90% of the flight lines flown on an aircraft equipped with kinematic GPS receivers for navigation as part of the PARCA initiative and provide a consistent data set of accurately geolocated measurements of ice thickness throughout Greenland.

The radar data reported here both complement and supplement previous data sets collected over the Greenland ice sheet [*Robin et al.*, 1969; *Ekholm*, 1996]. Also, *Bamber et al.* [this issue] developed a new ice thickness map by combining historical data with this new data set collected under the Program for Regional Climate Assesment (PARCA) initiative.

In this paper we provide a brief description of the system with emphasis on the new digital signal-processing section, antenna beam steering, and the *f-k* migration algorithm. We also provide sample results over the interior of the ice sheet where ice is about 3 km thick, from the 2000-m contour line in the south, and from two outlet glaciers: Storstrømmen Gletscher and Zachariae Isstrøm.

[1]Radar Systems and Remote Sensing Laboratory, The University of Kansas, Lawrence, Kansas.
[2]Jet Propulsion Laboratory, Pasadena, California.
[3]Department of Electrical Engineering, University of Missouri-Columbia, Columbia, Missouri.
[4]Byrd Polar Research Center, The Ohio State University, Columbus, Ohio.

Paper number 2001JD900183.
0148-0227/01/2001JD900183$09.00

Table 1. Important Radar System Parameters

Description	Characteristics	Unit
Center frequency	150	MHz
RF bandwidth	17	MHz
Waveform	chirped pulse	
Transmitter pulse width	1.6	μs
Compressed pulse width	60	ns
Range sidelobes	<26	dB
Peak transmitter power	200	W
Coherent integrations	32 to 4096	
Incoherent integrations	0 to 64000	
I and Q detector bandwidth	8.5	MHz
A/D dynamic range	72	dB
Antennas	four-element dipole array	
Sampling frequency	18.75	MHz
Sampling delay	0.080–300	μs
Range resolution in ice	4.494	m
Tx. feed network and cable losses	3	dB
Rx. cable and feed network losses	3	dB

2. System Description

A detailed description of the University of Kansas coherent radar system along with a few sample results is given by *Gogineni et al.* [1998]. Recently, we developed a new digital signal processor and incorporated antenna beam-steering circuits to improve the radar performance further. In this section we provide a brief description of the radar and the new digital system.

The coherent radars we used for collecting data over the Greenland ice sheet transmit a chirped pulse, which is linearly frequency modulated over a bandwidth of 17 MHz, of 1.6 μs duration, and has a peak transmit power of about 200 W. They use complementary surface acoustic wave (SAW) dispersive delay lines to generate the chirp signal and to compress the received signal. The compressed pulse width is about 60 ns. The antennas are two four-element dipole arrays mounted under each wing of the aircraft: one for transmission and the other for reception. To compensate for the aircraft wing tilt, the lengths of the cables driving each element were adjusted to cause the peak of the far-field radiation pattern from these arrays to occur directly beneath the aircraft.

Furthermore, to reduce the radiation sidelobes, the signal amplitudes of each element were modified according to a binomial weighting. This reduced the sidelobe level relative to the peak from about −13 dB for the uniformly weighted array to about −30 dB. The radar transmitter and receiver are mounted in a rack inside the aircraft and connected to their respective antennas with 20-m-long RF cables and a feed network with a combined loss of about 3 dB. The effective transmit power at the antenna is thus about 100 W.

A low-noise receiver with an overall gain of about 100 dB filters, amplifies, compresses, and coherently detects the received signal. The digital signal processor, consisting of two 12-bit A/D converters and adders, digitizes the in-phase (I) and quadrature (Q) output signals from the coherent detector and integrates them. The radar controller consists of circuits for generating delayed pulse repetition frequency and for setting the sampling window and the clock signal for the A/D converters. Table 1 provides important specifications of the system.

The radar system described by *Gogineni et al.* [1998] used the digital signal processor (DSP) developed in 1988 [*Xin*, 1989]. This DSP system used 8-bit A/D converters with a dynamic range of about 48 dB. It was housed in an external case that was connected to the host computer through a ribbon cable. This interface limited the data transfer rate between the DSP system and the host computer. A minimum of 150 coherent integrations at a pulse repetition frequency (PRF) of 4 kHz or less had to be performed by the DSP system before data could be transferred to the main computer, which limited the types of postprocessing that could be done.

To improve the system sensitivity, increase the dynamic range, and reduce the minimum number of onboard coherent integrations, we developed a new DSP system using 12-bit A/D converters and high-speed field-programable gate arrays (FPGAs). This allowed for fast integrations and reduction of the system's physical size. We developed the data acquisition card to interface with the PCI bus. Figure 1 shows the block diagram of the new DSP system. It consists of two cards that are plugged into a rack-mountable computer. One of these cards, designed to interface with PCI bus, digitizes the data and performs a number of coherent and incoherent integrations (if desired), and the other card generates PRF, the clock signal

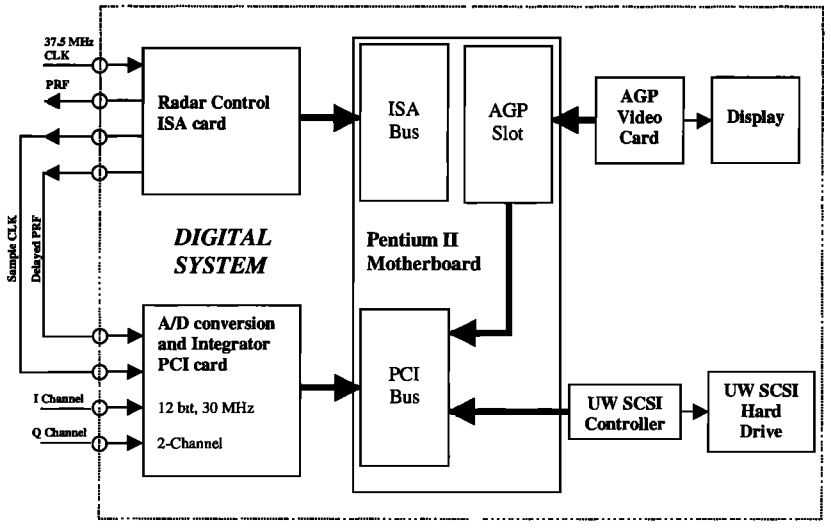

Figure 1. Block diagram of the radar digital signal processor.

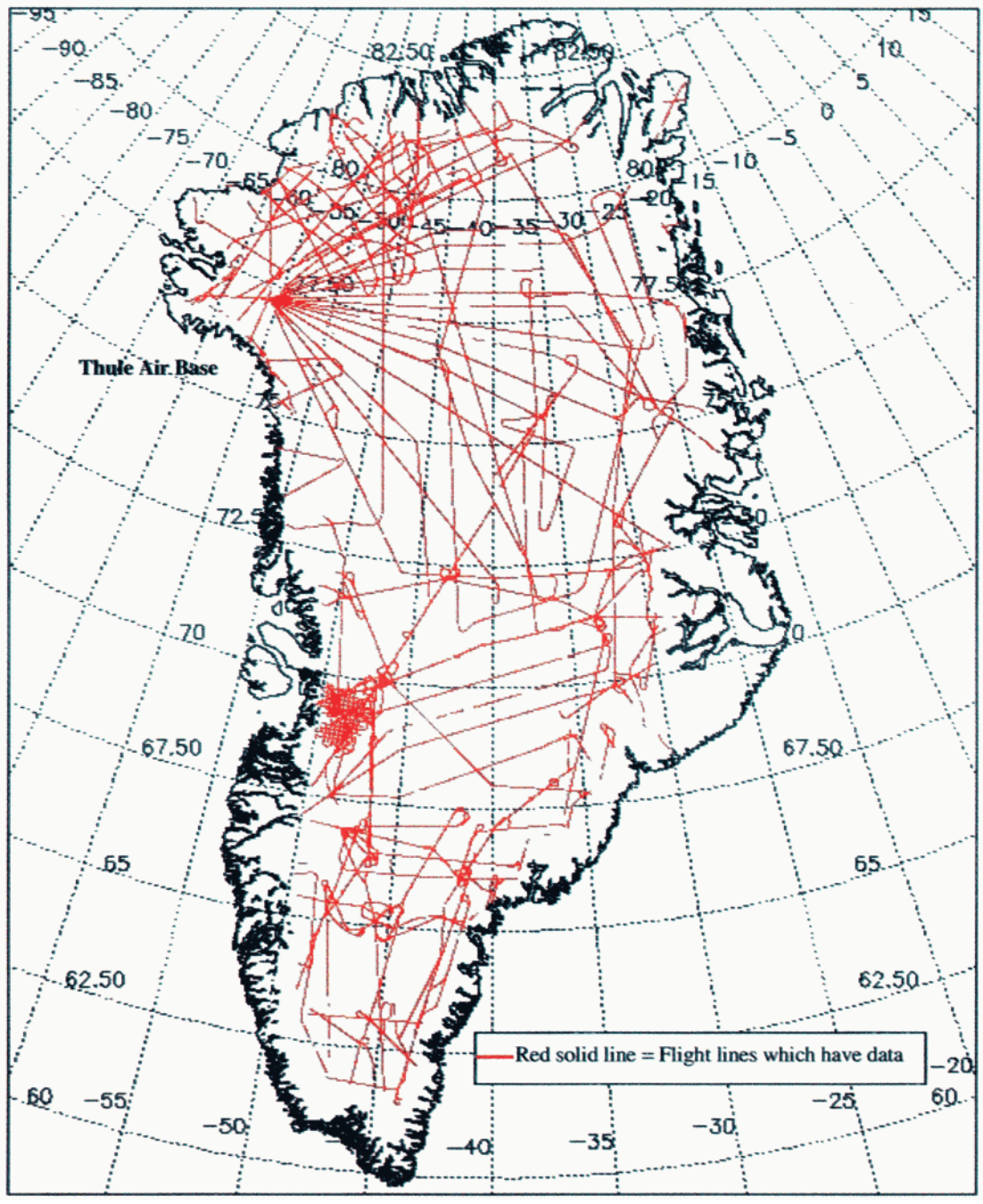

Plate 1. Locations of ice thickness data collected for Greenland with the University of Kansas radar depth sounder as part of the PARCA initiative. All measurements are accurately geolocated using kinematic GPS.

for the A/D converters, and the delayed PRF signal to start digitization. The host computer provides operator interface, stores digitized data on removable hard disks, and displays data in real time [*Akins*, 1999]. We used the new digital system to collect data during 1998 and 1999.

The new digital system is capable of collecting data with only 32 presummed coherent returns at a PRF of 9.2 kHz. It can also collect data over 2048 range bins and operate with a maximum PRF of 18.4 kHz, as opposed to 1024 range bins and a maximum PRF of 9.2 kHz for the old system. To operate with the higher PRF of 18.4 kHz, the number of range bins must be decreased to 800 (which corresponds to a maximum ice thickness of about 3 km for a radar operating at an altitude of 500 m over the ice surface), and the coherent presums must be increased to 64 or more. The new digital system also provides better gray-scale resolution (64 versus 4) of real-time data display for the operator. This allows the operator to make appropriate real-time receiver-gain adjustments to collect data in different parts of the ice sheet. We developed software that enables the operator to change radar parameters in flight and record onboard GPS location information and master clock data into every radar data record. The aircraft is normally flown in terrain-following mode at an altitude of about 450 m above the ice surface.

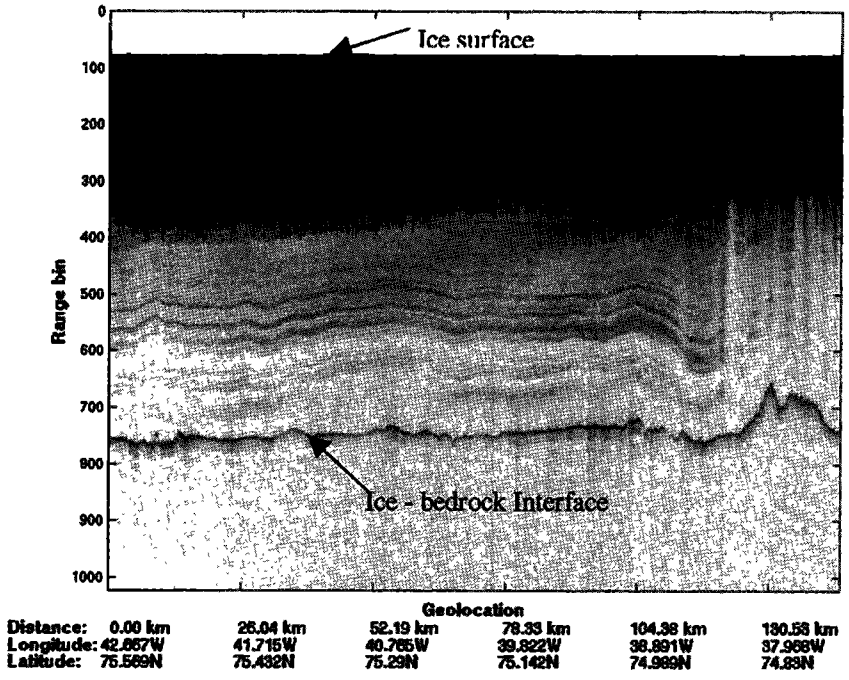

Figure 2a. Radar echogram from data collected over the interior of the ice sheet. (The radar data have been averaged over a distance covered by aircraft in 1 s (~130 m).)

3. Results

Since 1993, we have collected a large volume of ice thickness data as a part of the PARCA initiative. Reports with first-order results showing radar echograms and corresponding derived ice thicknesses for each flight line are provided both in electronic form (http://tornado.rsl.ukans.edu/Greenlanddata.htm) and in hard copy format [*Chuah et al.*, 1996a, 1996b; *Legarsky et al.*, 1997; *Wong et al.*, 1998; *Tee et al.*, 1999]. We estimated ice thickness by tracking the peaks of surface and ice-bedrock interface returns and by computing the number of range cells between the surface and the ice-bedrock interface peaks. We multiplied this number by 4.494, which is obtained by dividing free-space range-cell dimension by the refractive index of ice, to estimate ice thickness. Errors in the derived ice thickness have been estimated for several Greenland ice sheet locations. For high elevation, interior locations, we compared the radar-

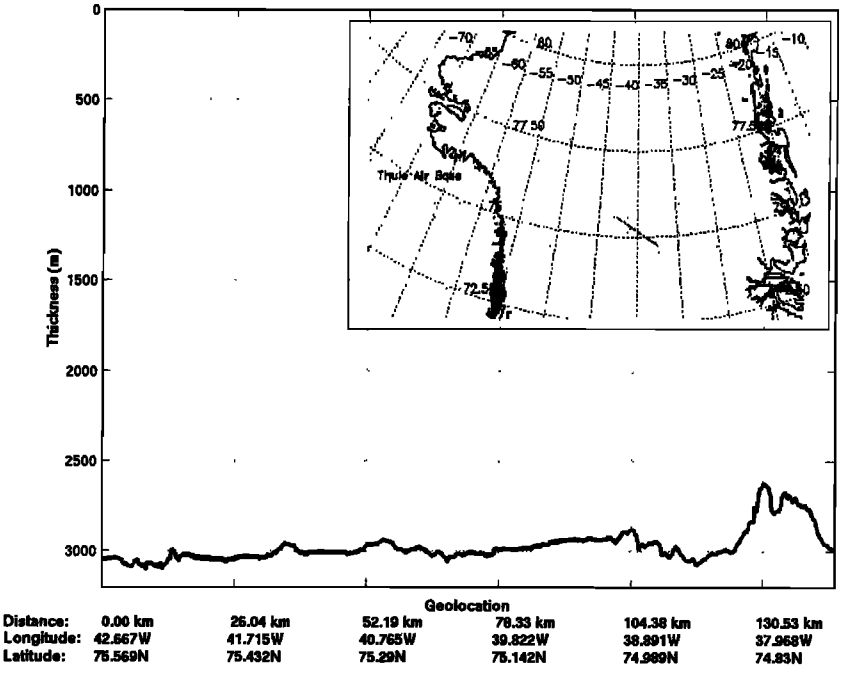

Figure 2b. Ice thickness obtained from radar data over the interior of the ice sheet. (The radar data have been averaged over a distance covered by aircraft in 1 s (~130 m).)

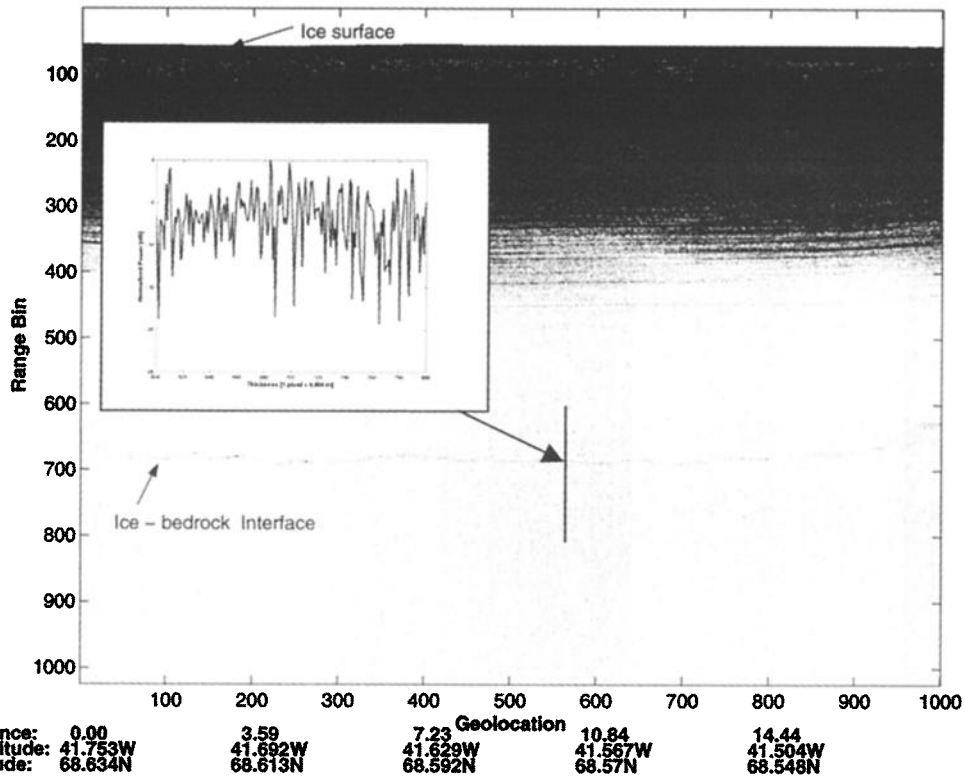

Figure 3a. Radar echogram from data collected over the central part of the ice sheet. (The radar data have been averaged over a distance covered by aircraft in ~0.139 s (~18 m).)

derived ice thickness information with GISP and GRIP cores. These results showed that radar-derived ice thicknesses were within ±10 m of that for these cores. We did not make any correction for firn effect, which could reduce this error further. For ice thickness measurements in the vicinity of outlet glaciers, *Luthi* [2000] measured ice thickness at two boreholes (828 and 831 m) on Jacobshaven Isbrae and found these measurements to be within a few meters of the radar-determined ice thickness of 830 m. Cross-point comparisons at seven locations in the vicinity of outlet glaciers (geolocation of ice thickness pairs separated by <75 m) gave an average absolute difference of 23.6 m.

We obtained good ice thickness data over 90% of the flight lines flown during PARCA, as shown in Plate 1. Our definition of good ice thickness data is that the signal-to-noise ratio for the bedrock echo is greater than 6 dB and is continuous over a distance of 20 km along the flight path. This is an extensive new data set in which all ice thickness data are accurately geolocated using kinematic GPS. We generated this plate by dividing the ice sheet into a grid with a resolution of 0.02° and 0.06° latitude and longitude, respectively. The grid extends from about 59.5° to 84° N in latitude and 75° to 10° W in longitude. We identified grid cells with valid thickness data or no data along each flight line. In this section we show a few examples of data collected over the interior of the ice sheet, around the margin, and on two outlet glaciers. We will show examples of data where we obtained good ice thickness data without any processing and where we applied the *f-k* migration algorithm to improve the signal-to-noise ratio.

Normally, we collected data with a radar PRF of 9.2 kHz and the integrator set to sum 256 samples coherently to reduce data volume. The aircraft was flown in terrain-following mode at an altitude of about 450 m above the ice surface with an airspeed of about 130 m/s. The distance traveled in the time to collect 256 samples at 9.2 kHz PRF is about 3.6 m. This distance is much less than an unfocused SAR aperture, which is about 21 m for a target located at a range of 450 m. We processed the data further by coherently integrating two to four samples and incoherently integrating 10–20 samples to reduce fading. Figures 2a and 2b show an example echogram and derived ice thickness for data collected and processed over the interior of the ice sheet. Ice thickness varies between 3.1 and 2.9 km over a distance of 100 km from the start of this flight segment. The bottom topography is relatively flat over the first 120 km, with a small peak of 400 m at the end. The S/N ratio for the bottom echo varies between 30 and 40 dB for the data shown in the figure. This confirms that the radar can provide consistent ice thickness information for more than 3 km of cold ice. Also, echoes associated with internal layers are visible to a depth of about 2.5 km. The white band between 100 and 200 pixels is the result of using a sensitivity time control (STC) circuit to prevent receiver saturation from the strong primary and multiple echoes from the air-ice interface.

For about 80% of the flight lines, we had to perform only a minimal amount of postprocessing (additional coherent integrations (two to four) and incoherent integrations (10–20) to reduce fading) to obtain good ice thickness data. Results over these lines are similar to those discussed above with the S/N ratio for bottom echoes varying between 10 and 40 dB. Because of increased absorption loss for warm ice over some areas in the south and central parts of the ice sheet, we had to perform additional postprocessing on these data using the *f-k* migration algorithm to extract ice thickness. *Gazdag and Sguazzero* [1984] and *Stolt* [1978] provide a detailed discussion

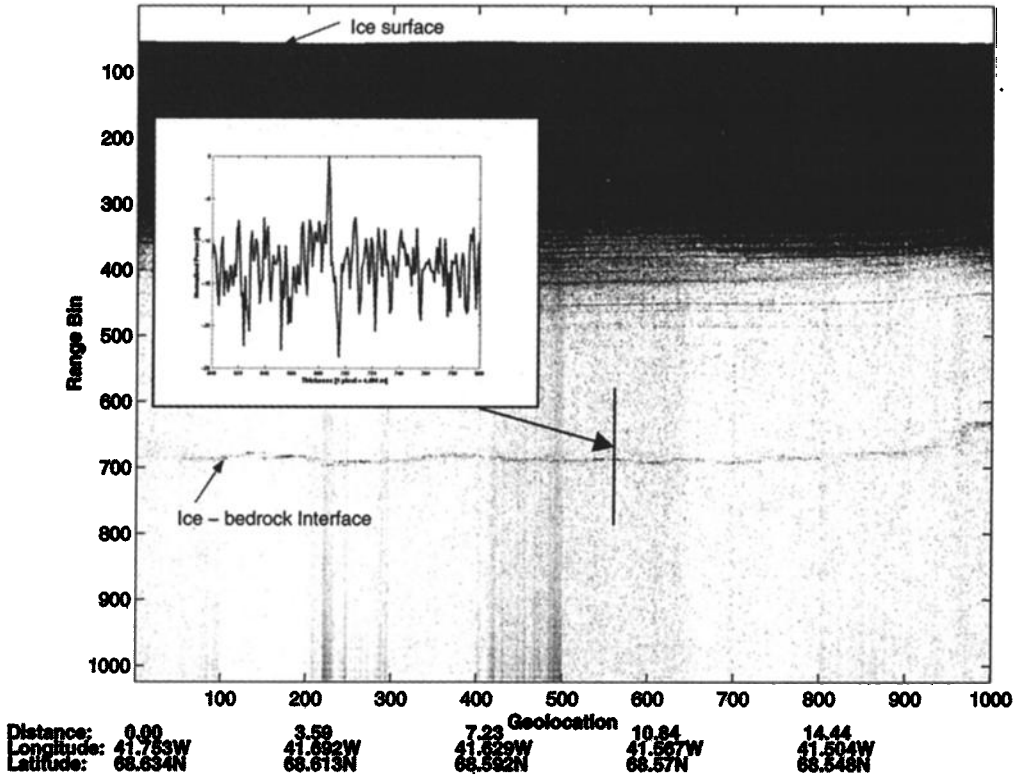

Figure 3b. Radar echogram from these data after processing with the *f-k* migration algorithm. (The radar data have been averaged over a distance covered by aircraft in ~0.139 s (~18 m).)

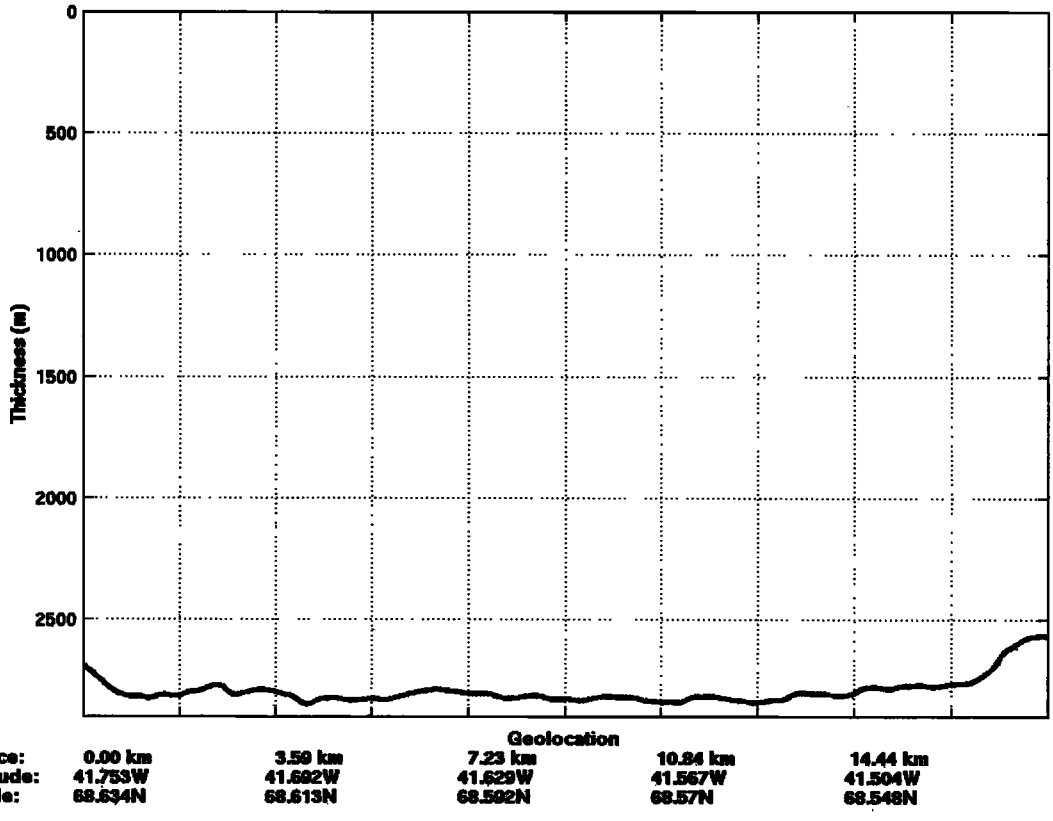

Figure 3c. Ice thickness obtained from the radar data collected over the central part of the ice sheet. (The radar data have been averaged over a distance covered by aircraft in ~0.139 s (~18 m).)

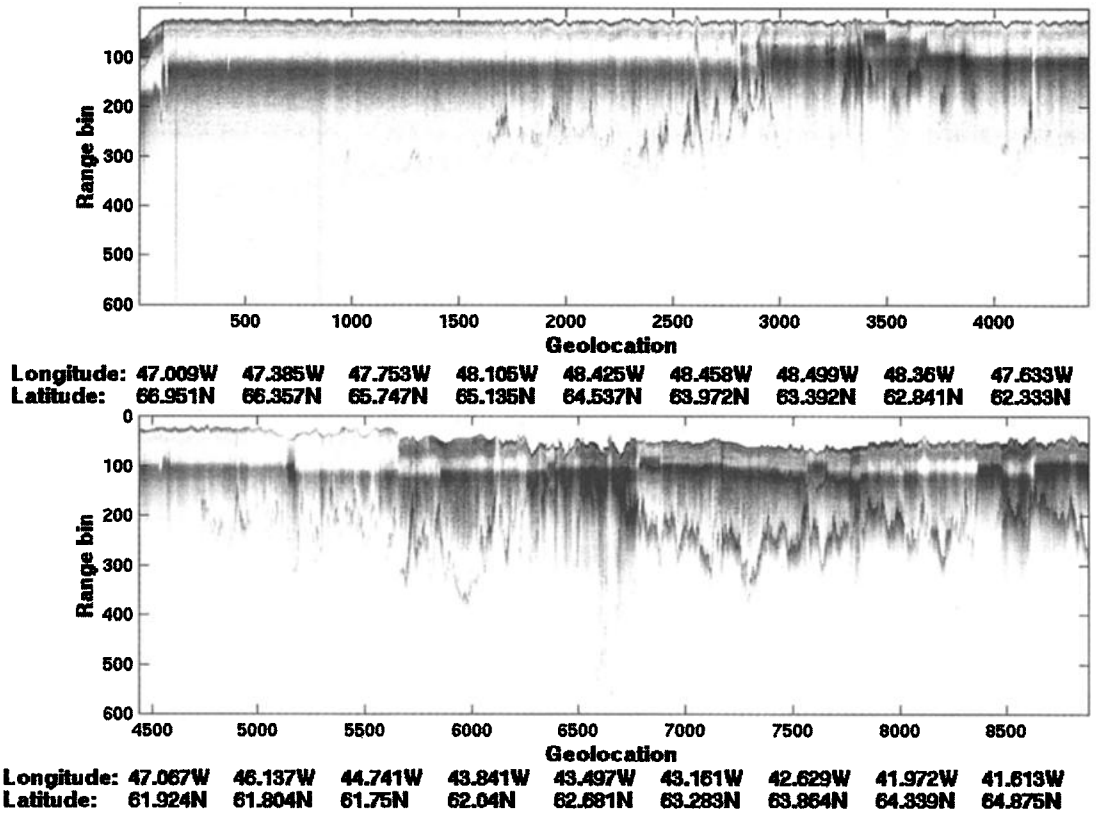

Figure 4. (a, b) Radar echograms of data collected along the 2000-m contour line in the south. (The radar data have been averaged over a distance covered by aircraft in 1 s (~130 m).)

of the *f-k* migration technique; therefore only a summary is provided here. The *f-k* migration algorithm is essentially a correlation processor (i.e., a matched filter) implemented with Fourier processing. The mathematics of this correlation processor can be interpreted as reverse migrating (i.e., reverse propagating) the received signals back to their sources (i.e., scatterers) within the ice. Thus the processing consists of a term that describes the migration of the received signal back to the air-ice interface, as well as a second term describing the propagation through the ice layer.

The coherent depth-sounding data received at the moving aircraft are denoted by $s_{rx}(t, x)$, which is a function both in time t and along-track distance x. Accordingly, these data can be represented in the frequency domain as

$$S_{rx}(\omega, k_x) = F\{s_{rx}(t, x)\}, \tag{1}$$

where F is the two-dimensional Fourier transform operator and ω and k_x are, respectively, the temporal and spatial Fourier frequency variables.

We then multiply this result with $H_{\text{air}}(\omega, k_x)$, the first term of the *f-k* migration algorithm,

$$S_{\text{surface}}(\omega, k_x) = H_{\text{air}}(\omega, k_x) S_{rx}(\omega, k_x) \tag{2}$$

where

$$H_{\text{air}}(\omega, k_x) = \exp(j2k_{za}h).$$

The value h is the height of the radar above the ice surface, and k_{za} is spatial frequency in the vertical z dimension. This value k_{za} is a function of both ω and k_x,

$$k_{za} = \sqrt{\frac{\omega^2}{c^2} - k_x^2}, \tag{3}$$

where c is the speed of electromagnetic propagation in air. The function $s_{\text{surface}}(\omega, k_x)$ can be interpreted as the Fourier transform of $s_{\text{surface}}(x, t)$, the scattered (scalar) wave on the ice surface. In other words, $H_{\text{air}}(\omega, k_x)$ migrates the received signal from the radar back to the ice surface.

The next term of the *f-k* migration process further backpropagates this wave, down through the ice layer to a depth d.

$$S_{\text{ice}}(\omega, k_x) = H_{\text{ice}}(\omega, k_x) S_{\text{surface}}(\omega, k_x), \tag{4}$$

where

$$H_{\text{ice}}(\omega, k_x) = \exp(j2k_{zi}d)$$

In the ice the spatial frequency variable k_{zi} is expressed as

$$k_{zi} = \sqrt{\frac{\omega^2}{v_{\text{ice}}^2} - k_x^2}, \tag{5}$$

where v_{ice} is the velocity of electromagnetic propagation within the ice, in this case a value-assumed constant.

The inverse Fourier transform of $s_{\text{ice}}(\omega, k_x)$ again can be interpreted as the signal $S_{\text{ice}}(t, x)$ at a depth d under the ice surface. Recall that *f-k* migration is effectively a correlation processor, and a correlation operation can be implemented by evaluating the output of a matched filter at a specific time. Similarly, a two-dimensional subsurface image, $u(x, z)$, is generated in *f-k* migration by evaluating $s_{\text{ice}}(t, x)$ at a specific time τ.

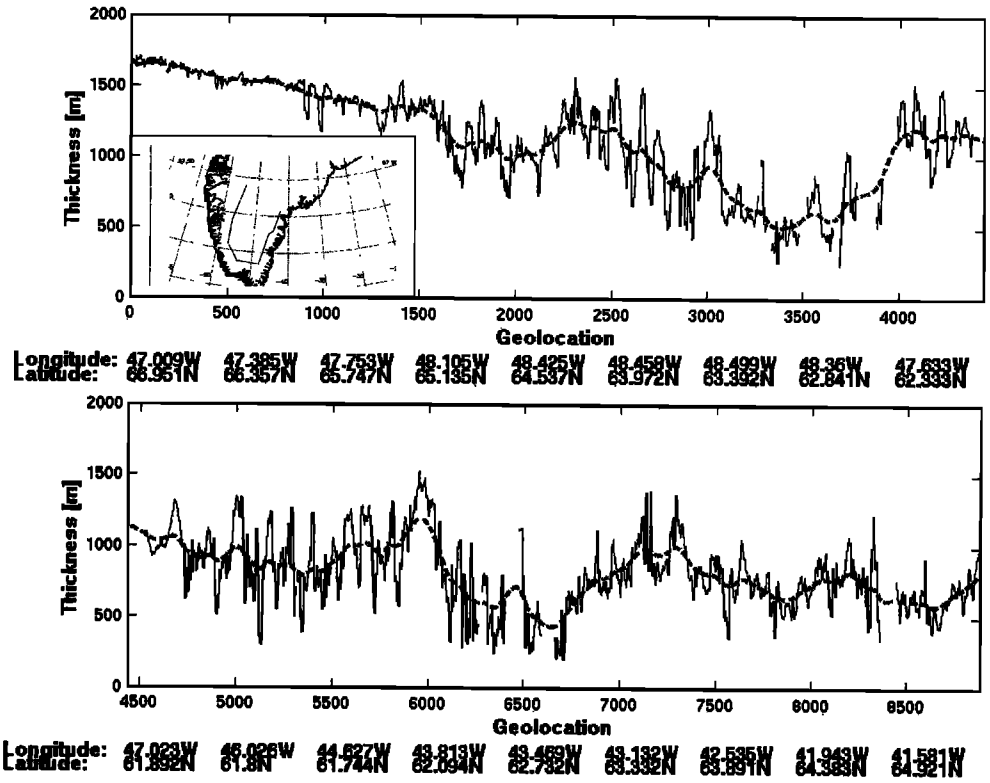

Figure 4. (c, d) Ice thickness obtained from radar data along the 2000-m contour line in the south. (The radar data have been averaged over a distance covered by aircraft in 1 s (~130 m).)

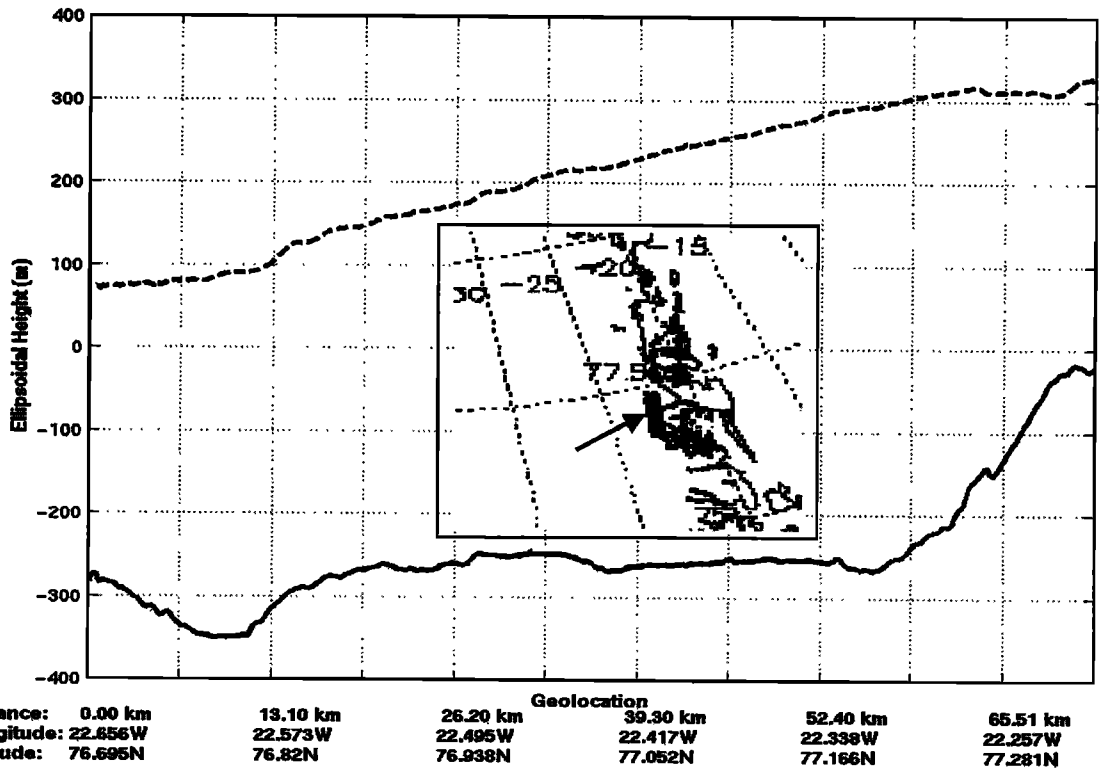

Figure 5a. Ice surface elevation and ice bottom elevation (WGS84 ellipsoid) along a flight up Storstrømmen Gletscher on May 24, 1997. (The radar data have been averaged over a distance covered by aircraft in 1 s (~130 m).)

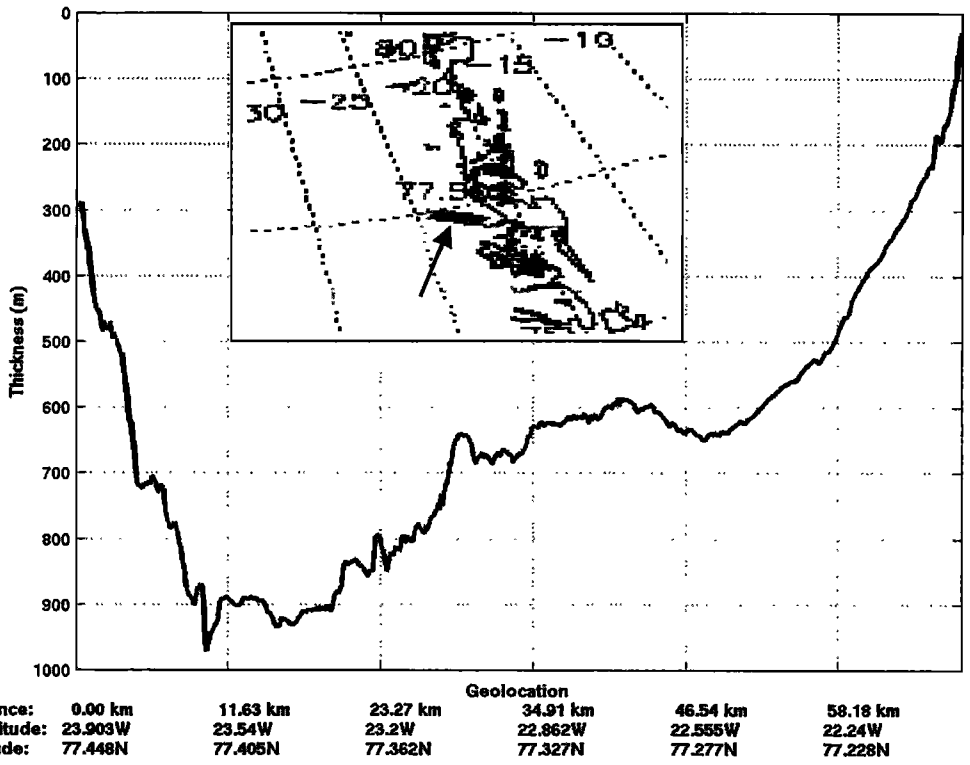

Figure 5b. Ice thickness along a flight across Storstrømmen Gletscher on May 22, 1996. (The radar data have been averaged over a distance covered by aircraft in 1 s (~130 m).)

$$u(x, z = -d) = s_{\text{ice}}(t = \tau, x). \tag{6}$$

The value $t = \tau$ can be interpreted as the time when $s_{\text{ice}}(t, x)$ represents the wave energy due to scattering specifically from depth d, as opposed to later times ($t > \tau$) where $s_{\text{ice}}(t, x)$ will be due to the scattered energy from lower layers that have propagated up to depth d.

A complete subsurface image $u(x, z)$ can thus be constructed using f-k migration by calculating and evaluating $s_{\text{ice}}(t, x)$ at all depths $z = -d$. Figures 3a and 3b show radar echograms generated with normal processing and the f-k migration algorithm. The inset in these figures shows the amplitude of echoes as a function of depth. Corresponding ice thicknesses for this echogram are plotted in Figure 3c. The S/N ratio for the bottom echo using conventional data processing is about 4 dB, whereas the S/N ratio for data processed with the f-k migration algorithm is 10 dB. Over the entire image we obtained a 4–6 dB improvement in the S/N ratio for data processed with the f-k algorithm over that obtained with conventional processing.

We only processed data with weak bottom echoes with f-k migration because it is computationally intensive. We obtained good thickness information for about an additional 10% for the flight lines beyond the 80% obtained with conventional processing. The areas where we could not obtain ice thickness consisted primarily of the deep, narrow channel beneath the Jacobshavn outlet glacier and near the margins of the ice sheet where bottom echoes were merged with multiples of the ice surface. Much of the radar data over the Jacobshavn area were collected in incoherent mode during 1997, and we could not postprocess these data to improve the S/N ratio. We believe that we can obtain ice thickness within the narrow channel with these radars if the measurements are made in coherent mode before a significant surface melt starts and near the ice sheet margins with the aircraft flown at different altitudes for the remaining 10% of the flight lines.

Figures 4a and 4b show radar echograms and Figures 4c and 4d show derived ice thicknesses along the 2000-m contour line in the south. We collected these data with a radar PRF of 15 kHz and the integrator set to presum 128 returns coherently. We postprocessed recorded data by coherently integrating four presummed returns and incoherently summing 30 coherently integrated returns. With an airspeed of about 130 m/s, spacing between points along the x axis is ~130 m. We low-pass filtered the derived ice thickness data and plotted the average ice thickness obtained after low-pass filtering, shown as a dashed line in Figures 4c and 4d. Ice thickness gradually decreased from about 1700 m at the start of the flight line (inset in Figure 4c) to about 1500 m over the first 100 km. It then decreased rapidly from about 1500 m to about 600 m over the next 350 km with significant surface relief. The maximum peak-to-peak ice thickness deviation is about 800 m in this region. The small gap in ice thickness between 3500 and 3700 units is caused by weak bottom echoes submerged in clutter from off-angle surface returns and ice-surface multiples. The average ice thickness increased from about 500 to 1200 m over the next 10 km, and then it decreased gradually from 1200 to 800 m over the next 200 km. Bottom topography is very rough in this area with peak-to-peak deviations of about 700 m over a distance of about 10 km. We believe that these are the first high-quality ice thickness data collected over this region of the ice sheet.

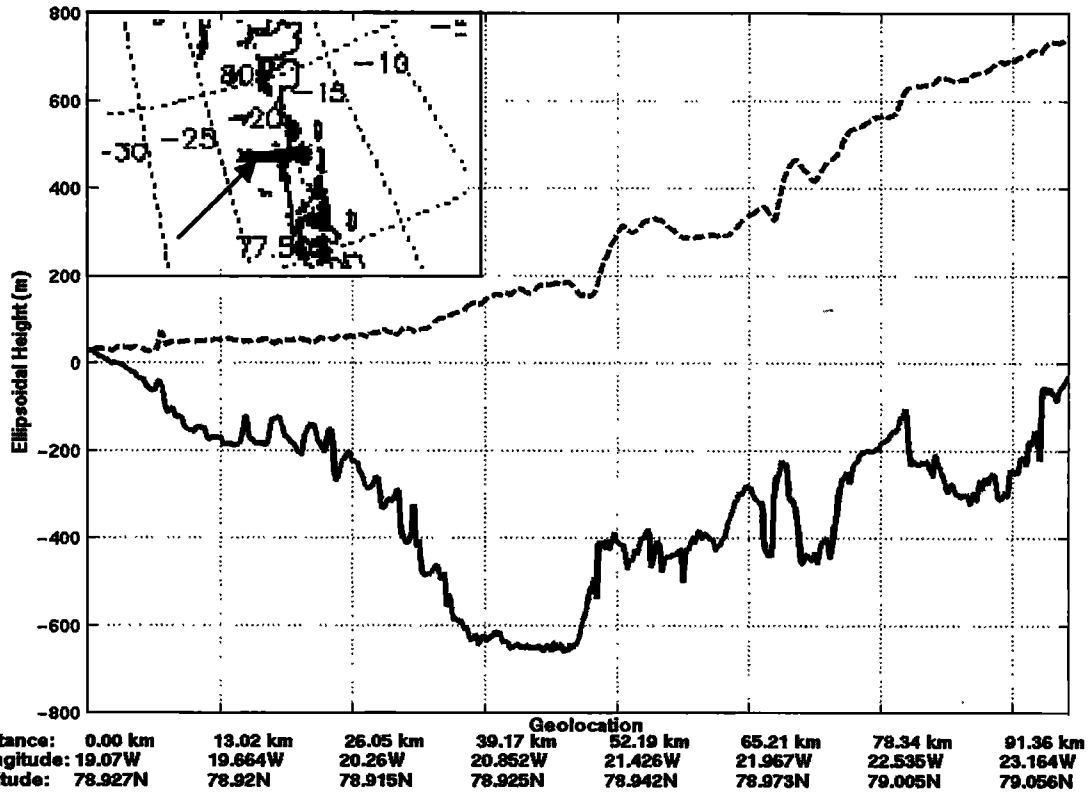

Figure 6a. Ice surface elevation and ice bottom elevation (WGS84 ellipsoid) along a flight up Zachariae Isstrøm on May 19, 1999. (The radar data have been averaged over a distance covered by aircraft in 1 s (~130 m).)

3.1. Outlet Glaciers

Along the Greenland ice sheet margin, outlet glaciers play a major role in ice discharge and account for about half of the total mass loss from the ice sheet [*Reeh et al.*, 1999]. Ice thickness measurements obtained from the coherent radar depth sounder in conjunction with high-resolution surface images (e.g., Landsat and satellite synthetic aperture radar (SAR)), permit three-dimensional characterizations of the outlet glaciers. Surface images provide important information on the lateral surface dimensions of outlet glaciers, the location of the calving front, the surrounding topography, and ice surface flow lines. Surface images can also be used to determine the ice flow velocity, and *Rignot et al.* [1997] have used interferometric SAR to determine the surface velocity of outlet glaciers with an accuracy of about 1 m yr^{-1}. Radar ice thickness measurements provide the critical third dimension that allows assessment of volume flux, bed topography, and the locations of grounding lines. The grounding line location is an especially important parameter in assessing mass balance since subglacial melting of floating ice can be large [*Reeh et al.*, 1997; *Mayer et al.*, 2000].

Using GPS-derived positions associated with the radar ice thickness measurements and the corresponding ice surface elevation measurements from the airborne topographic mapper (ATM), flight paths over outlet glaciers were plotted on high-resolution SAR images using the National Snow and Ice Data Center (NSIDC) LIMB (large image map browser) software. NSIDC distributes this software to view the digital SAR mosaic of the Greenland ice sheet that was compiled from ERS-1 data obtained during August 1992. This allows the radar ice thickness and ATM ice surface elevation measurements to be placed in proper context with the local complex terrain. We present detailed characterizations of two example outlet glaciers located in northeast Greenland: Storstrømmen Gletscher (77.0° N, 22.6° W) and Zachariae Isstrøm (79.0° N, 20.0° W). For each of these outlet glaciers, ice thickness profiles along the glacier axis and across the glacier are presented. Also included are crossover points to quantify the repeatability of these measurements.

Storstrømmen Gletscher is roughly oriented in the north-south direction and is ~41 km wide in the entrance region, narrowing to ~24 km in the main channel. *Weidick* [1995] gives the speed of this glacier as ranging from 200 to 1800 m yr^{-1}. Figure 5a shows ice surface elevation and ice bottom elevation (WGS84 ellipsoid) from a flight on May 24, 1997, which began inland of the calving front and over the center of the glacier axis. The flight trajectory was up the glacier at a slightly off-axis angle that took it within about 8 km of its eastern boundary. Initially, the ice thickness (obtained by subtracting the ice bottom elevation from the ice surface elevation) increased by 85 m to ~440 m at a distance of about 9.5 km along the flight path, due to a decrease in the ice base elevation. The ice thickness decreased slightly to 415 m between 9.5 and 19 km due mainly to an increase in ice base elevation. Ice thickness then increased at a rate of about 3.76 m km^{-1} to ~550 m over the next 40 km as the ice surface elevation increased and the bed elevation remained nearly constant at approximately −250 m. Beyond this point, the bed elevation increased as the flight trajectory left the main glacial channel.

As seen in Figure 5a, the bed topography of Storstrømmen

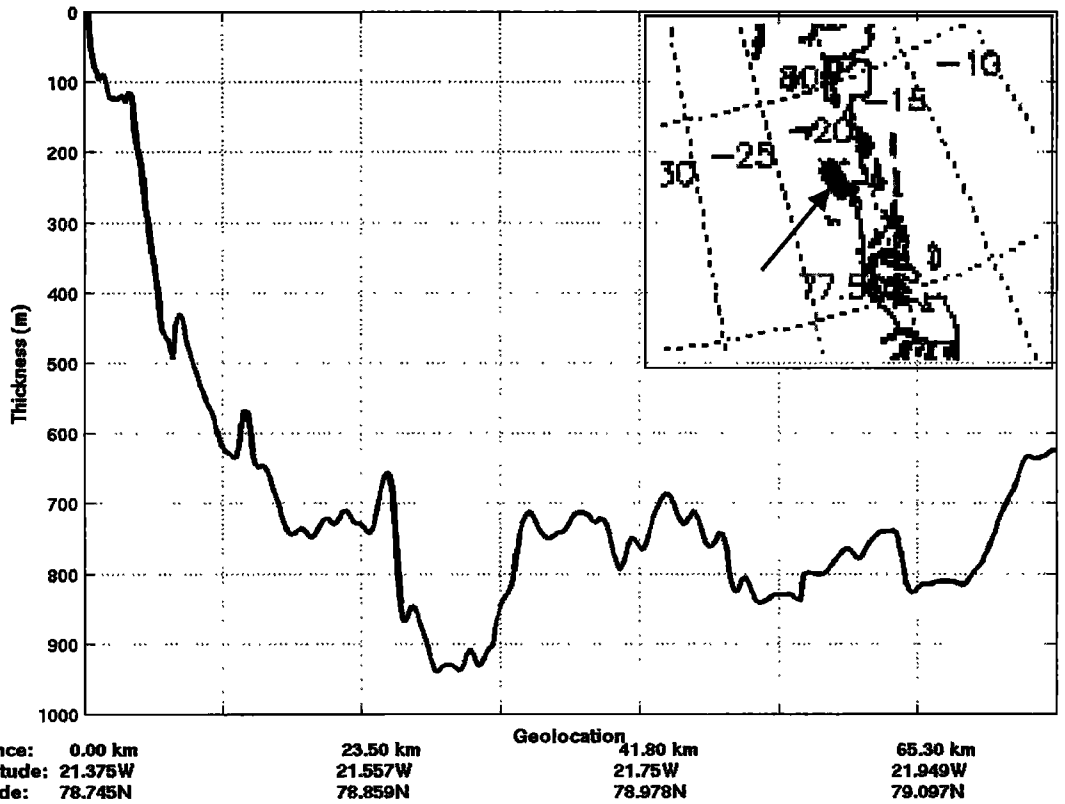

Figure 6b. Ice thickness along a flight across Zachariae Isstrøm on May 24, 1997. (The radar data have been averaged over a distance covered by aircraft in 1 s (~130 m).)

Gletscher was quite smooth. Figure 5b shows ice thickness from a flight on May 22, 1996, having a trajectory across the entrance region of Storstrømmen Gletscher from the west to the east side. The western portion of the glacier basin was the deepest, with an ice thickness of more than 800 m extending over ~19 km. The eastern half of the glacier entrance region had a thickness averaging 632 m. A crossover point in the two flights described above was compared, showing very close agreement in the ice thickness measurements. The 1997 up-glacier flight measured an ice thickness of 530.0 m, and the 1996 cross-glacier flight measured an ice thickness of 529.7 m at roughly the same GPS location.

Zachariae Isstrøm is roughly oriented in the east-west direction. This glacier is ~60 km wide in the entrance region, narrowing to ~26 km over a distance down the glacier of ~35 km. *Weidick* [1995] states that the speed of this glacier is 500 m yr^{-1}. Figure 6a shows the ice surface elevation and the ice base elevation from a flight on May 19, 1999, which began over floating ice and continued up the center of the glacier axis. The ice thickness increased from zero (ice surface elevation is equal to the ice bed elevation) to ~250 m in the bay beyond the exit region of the glacier at a point about 25 km along the flight path. Beyond this, thickening rapidly occurred primarily due to a large decrease in the ice bed elevation and a moderate increase in ice surface elevation between 25 km and 40 km. Along this 15-km segment of the flight path, ice thickness increased at a rate of about 39.1 m km^{-1} to ~810 m, a thickening rate that is more than 10 times of what was observed for Storstrømmen Gletscher. The 40 km point along the flight path corresponds to the smallest lateral extent of the glacier.

It is also apparent from Figure 6a that the bed topography of Zachariae Isstrøm is very rough in comparison with Storstrømmen Gletscher. Figure 6b shows ice thickness from a flight on May 24, 1997, having a trajectory across the entrance region of Zachariae Isstrøm from the south to the north. The average ice thickness across the main glacier bed was 770 m, with the deepest portion of the glacier basin having an ice thickness of more than 900 m. A crossover point for these two flights also shows good agreement. The 1999 up-glacier flight measured an ice thickness of 712.6 m, and the 1997 cross-glacier flight measured an ice thickness of 727.1 m at roughly the same GPS location. This is consistent with ±10 m accuracy inferred from the comparison of radar-derived thicknesses to GISP and GRIP ice cores.

4. Conclusions

We have developed two coherent radars for measuring ice thickness and have conducted extensive aircraft surveys compiling a large, consistent, geolocated data set of ice thickness on the Greenland ice sheet as part of the NASA PARCA initiative. These radars obtain the high sensitivity required to sound glacial ice more than 3 km thick using pulse compression and coherent signal processing while transmitting at only about 200 W peak power. We obtained good ice thickness information for over 80% of the flight lines flown as a part of the PARCA initiative with normal postprocessing plus an additional 10% of the flight lines using the f-k migration algorithm. We have presented examples of data from the interior, over the margins and on the outlet glaciers of the Greenland ice sheet, which demonstrate the widely varying bedrock topography for different regions of the ice sheet. We distribute these

data to the scientific community both in hard copy form and in electronic form from our server. The development of these radars involved significant participation by Electrical Engineering and Computer Science undergraduate students as a part of their education.

Notation

s = received radar signal as a function of time and distance.
S = received radar signal as a function of frequency and distance.
$S_{\text{surface}}(\omega, k_x)$ = Fourier transform of $s_{\text{surface}}(x, t)$, the scattered (scalar) wave on ice surface.
H_{air} = matched filter response for a target on the surface.
H_{ice} = matched filter response for a target on the ice.
t = time.
x = distance.
F = two-dimensional Fourier transform operator.
ω = temporal frequency variable.
k_x = spatial frequency wave number in x direction.
h = height of radar above ice surface.
k_{za} = spatial frequency in vertical dimension, z, in air.
k_{zi} = spatial frequency variable in vertical dimension, z, in ice.
c = speed of electromagnetic propagation in air.
d = depth.
v_{ice} = velocity of electromagnetic propagation within ice.
$u(x, z)$ = two-dimensional subsurface image.
τ = specific time.

Acknowledgments. The work is supported by NASA grant NAG5-8758. We would like to thank William Krabill from the NASA Goddard Space Flight Center for providing surface elevation data and Doug Young, also from Goddard, who designed the antenna mount. We thank the aircraft crew for the excellent support provided while conducting these experiments. We also acknowledge Greg Rosen and Meng Wu for their help in plotting flight trajectories and Donnis Graham for editing this paper. The analyses of outlet glaciers presented in this paper benefited greatly from the digital SAR mosaic of the Greenland ice sheet produced by Mark Fahnestock (Department of Meteorology, University of Maryland, College Park) and Ron Kwok (Jet Propulsion Laboratory, California Institute of Technology, Pasadena). The helpful suggestions and comments of two reviewers are also greatly appreciated.

References

Akins, T., Design and development of an improved data acquisition system for the coherent radar depth sounder, M.S. thesis, Electr. Eng. and Comput. Sci., Univ. of Kansas, Lawrence, Kansas, 1999.

Bamber, J. L., R. L. Layberry, and S. P. Gogineni, A new ice thickness and bed data set for the Greenland ice sheet, 1, *J. Geophys. Res.*, this issue.

Chuah, T. S., S. Gogineni, C. Allen, B. Wohletz, Y. C. Wong, P. Y. Ng, and E. Ajayi, Radar thickness measurements over the southern part of the Greenland ice sheet [1993 data], *RSL Tech. Rep. 10470-2*, Radar Syst. and Remote Sens. Lab., Univ. of Kansas, Lawrence, Kansas, 1996a.

Chuah, T. S., S. Gogineni, C. Allen, and B. Wohletz, Radar thickness measurements over the northern part of the Greenland ice sheet [1995 data], *RSL Tech. Rep. 10470-3*, Radar Syst. and Remote Sens. Lab., Univ. of Kansas, Lawrence, Kansas, 1996b.

Ekholm, S., A full coverage, high-resolution topographic model of Greenland composed from a variety of digital elevation data, *J. Geophys. Res.*, *101*, 21,961–21,972, 1996.

Gazdag, J., and P. Sguazzero, Migration of seismic data, *Proc. IEEE*, *72*, 1302–1315, 1984.

Gogineni, S., T. Chuah, C. Allen, K. Jezek, and R. K. Moore, An improved coherent radar depth sounder, *J. Glaciol.*, *44*, 659–669, 1998.

Legarsky, J., S. P. Gogineni, C. Allen, T. S. Chuah, and Y. C. Wong, Radar thickness measurements over the northern part of Greenland ice sheet—1996 results, *RSL Tech. Rep. 10470-6*, Radar Syst. and Remote Sens. Lab., Univ. of Kansas, Lawrence, Kansas, 1997.

Luthi, M. P., Rheology of cold frin and dynamics of a polythermal ice stream, Ph.D. dissertation, Eidg. Tech. Hochsch., Zurich, Switzerland, 2000.

Mayer, C., N. Reeh, F. Jung-Rothenhäusler, P. Huybrechts, and H. Oerter, The subglacial cavity and implied dynamics under Nioghalvfjerdsfjorden Glacier, NE-Greenland, *Geophys. Res. Lett.*, *27*(15), 2289–2292, 2000.

Raju, G., W. Xin, and R. K. Moore, Design, development, field operations and preliminary results of the coherent Antarctic radar depth sounder (CARDS) of the University of Kansas, USA, *J. Glaciol.*, *36*, 247–258, 1990.

Reeh, N., H. Thomsen, O. Olesen, and W. Starzer, Mass balance of North Greenland, *Science*, *278*, 205–206, 1997.

Reeh, N., C. Mayer, H. Miller, H. Thomsen, and A. Weidick, Present and past climate control on fjord glaciations in Greenland: Implications for IRD-deposition in the sea, *Geophys. Res. Lett.*, *26*(8), 1039–1042, 1999.

Rignot, E. J., S. P. Gogineni, W. B. Krabill, and S. Ekholm, North and northeast Greenland ice discharge from satellite radar interferometry, *Science*, *276*, 934–937, 1997.

Robin, G. de O., S. Evans, and J. T. Bailey, Interpretation of radio echo sounding in polar ice sheets, *Philos. Trans. R. Soc. London, Ser. A*, *265*, 437–505, 1969.

Stolt, R. H., Migration by Fourier transform, *Geophysics*, *43*, 23–48, 1978.

Tee, K. L., W. K. Chong, H. Coulter, T. Akins, S. P. Gogineni, C. Allen, and J. Stiles, Radar thickness measurement over the southern part of the Greenland ice sheet—1998 results, *RSL TR 13720-10*, Radar Syst. and Remote Sens. Lab., Univ. of Kansas, Lawrence, Kansas, 1999.

Weidick, A., Greenland [with a section of Landsat images of Greenland by R. S. Williams Jr. and J. G. Ferrigno], in *Satellite Image Atlas of Glaciers of the World*, edited by R. S. Williams Jr. and J. G. Ferrigno, *U.S. Geol. Surv. Prof. Pap. 1386-C*, 141 pp., Washington, D. C., 1995.

Wong, Y. C., S. Gogineni, C. Allen, J. Stiles, J. Legarsky, T. Akins, and K. L. Tee, Radar thickness measurements over the Greenland ice sheet—1997 results, *RSL Tech. Rep. 10470-7*, Radar Syst. and Remote Sens. Lab., Univ. of Kansas, Lawrence, Kansas, 1998.

Xin, W., Data processing system of the coherent Antarctic radar depth sounder, *RSL Tech. Rep. 8070-3*, Radar Syst. and Remote Sens. Lab., Univ. of Kansas, Lawrence, Kansas, 1989.

C. Allen, D. Braaten, P. Gogineni, P. Kanagaratnam, C. Leuschen, J. Stiles, and D. Tammana, Remote Sensing Laboratory, University of Kansas, 2335 Irving Hill Road, Lawrence, KS 66045-7612. (gogineni@rsl.ukans.edu)

T. Akins, Jet Propulsion Laboratory, 4800 Oak Grove Dr., Pasadena, CA 91109.

K. Jezek, Byrd Polar Research Center, The Ohio State University, 108 Scott Hall, 1090 Carmack Road, Columbus OH 43210-1002.

J. Legarsky, Department of Electrical Engineering, University of Missouri-Columbia, 223 Engineering Building West, Columbia, MO 65211.

(Received July 31, 2000; revised February 5, 2001;
accepted February 15, 2001.)